Article

Voltage Differencing Buffered Amplifier-Based Novel Truly Mixed-Mode Biquadratic Universal Filter with Versatile Input/Output Features

Mohammad Faseehuddin [1], **Norbert Herencsar** [2], **Sadia Shireen** [1], **Worapong Tangsrirat** [3] **and Sawal Hamid Md Ali** [4,*]

1 Department of Electronics & Telecommunication, Symbiosis Institute of Technology, Symbiosis International (Deemed University), Lavale, Pune 412115, Maharashtra, India; mohammad.faseehuddin@sitpune.edu.in (M.F.), sadia.shireen.phd2021@sitpune.edu.in (S.S.)
2 Department of Telecommunications, Faculty of Electrical Engineering and Communication, Brno University of Technology, Technicka 3082/12, 61600 Brno, Czech Republic; herencsn@ieee.org
3 Department of Instrumentation and Control Engineering, School of Engineering, King Mongkut's Institute of Technology Ladkrabang (KMITL), Bangkok 10520, Thailand; worapong.ta@kmitl.ac.th
4 Department of Electrical, Electronic and Systems Engineering, Universiti Kebangsaan Malaysia, Bangi 43600, Selangor, Malaysia
* Correspondence: sawal@ukm.edu.my; Tel.: + 60-3-8911-8393

Abstract: In this paper, a first-of-a-kind mixed-mode universal filter employing three VDBAs and three passive components, is proposed. The filter operates in all four modes and provides all five filter responses, namely voltage-mode (VM), current-mode (CM), trans-impedance-mode (TIM), or trans-admittance-mode (TAM). Additionally, the same filter topology can also work as a CM single-input-multi-output (SIMO) filter. A state-of-the-art comparison of various 'voltage differencing' variants of the voltage differencing buffered amplifier (VDBA)-based SIMO/MISO (single-input-multi-output/multi-input-single-output)-type biquad filters further highlight the significance of the presented research. In the proposed no passive component matching is required for generating the filter responses. The filter circuit also provides inbuilt tunability of the quality factor independent of the pole frequency. The non-ideal frequency dependent gain and component sensitivity analyses of the filter were also performed. The Silterra Malaysia 0.18 μm process design kit (PDK) is employed to design and validated the proposed VDBA-based filter using the Cadence design software. The simulation results closely follow the theoretical predictions. To further verify the practical feasibility of the proposed filter, an experimental evaluation is also completed. The VDBA-based filter is implemented using off-the-shelf operational transconductance amplifiers Intersil CA3080, Texas Instruments LF356 op-amp, and Analog Devices AD844s. The filter is designed for a characteristic frequency of 100 kHz. The time and frequency domain measurement results indicate the proper functioning of the filter.

Keywords: analog signal processing; filters; mixed-mode; voltage differencing buffered amplifier; VDBA

1. Introduction

Analog frequency filters are an important component of signal processing system. They are employed in instrumentation systems, communication systems, speech processing, sensor data preprocessing, data acquisition systems, etc. [1–3]. The active element-based filters are the most employed as they have advantages in terms of chip area, low-power operation, tunability, and compatibility [1,2]. In present day complex signal processing systems, as the design complexity of the system is increasing to achieve high performance, both current-mode and voltage-mode signal processing circuits are employed in a single system. In order to connect the current-mode output to a voltage-mode circuit or vice versa,

trans-admittance and trans-impedance stages are required to perform voltage to current (V-I) and I-V conversion. The mixed-mode filters will find application in such a scenario as it will perform the dual task of signal processing and signal conversion simultaneously. One such example is given in reference [4] of a three-way high-fidelity loudspeaker crossover network. The design of mixed-mode universal filters that can provide low-pass (LP), high-pass (HP), band-pass (BP), band-reject (BR), and all-pass (AP) filter responses in CM, VM, TAM, and TIM modes of operation are needed for the mixed signals system architecture [1,2,5–20]. The popular analog building blocks (ABBs) that are used in the design of active filters include operational transconductance amplifier (OTA) [5], second-generation current conveyor (CCII) [6], differential voltage current conveyor (DVCC) [16], extra current conveyor transconductance amplifier (EXCCTA) [21], differential difference current conveyor (DDCCII) [18], fully differential current conveyor (FDCCII) [15], current differencing buffer amplifier (CDBA) [3], etc. The voltage differencing buffered amplifier (VDBA) is another popular ABB that is very simple in design and versatile in realizing numerous applications [3,22–24]. Various 'voltage differencing' variants of the VDBA are proposed, such as fully balanced voltage differencing buffered amplifier (FB-VDBA) [25], voltage differencing inverting buffered amplifier (VDIBA) [26,27], fully balanced voltage differencing inverting buffered amplifier (FB-VDIBA) [28], or voltage differencing differential input buffered amplifier (VD-DIBA) [29]. In Tables 1 and 2, a comparative study is carried out to compare the state-of-the-art SIMO/MISO (single-input-multi-output/multi-input-single-output) voltage differencing unit (VDU)-based biquad filters [25,26,28–53] with here proposed designs. The comparison is made based on the following relevant criteria:

(i)   Number of ABBs employed;
(ii)   Count of passive components used;
(iii)   A requirement of passive components matching condition;
(iv)   Application of negative input for response generation;
(v)   A requirement of double voltage input for response realization;
(vi)   Low output impedance in the case of VM and TIM filters;
(vii)   High output impedance in the case of CM and TAM filters;
(viii) Mode of operation;
(ix)   Independent tunability of quality factor and filter frequency;
(x)   Can realize all five filter responses;
(xi)   Test frequency;
(xii)   Power dissipation;
(xiii) Supply voltage;
(xiv)   Total harmonic distortion (THD).

Reported VDBA-based universal biquadratic filters have three major limitations that severely curtail their application spectrum, which are: (a) non-availability of all five filter responses, (b) the employment of floating passive components, and (c) passive component matching constraints. It can be inferred from the comparative study that out of the 30 designs available in the literature; only 15 can provide all five filter responses in either VM and CM mode [23,26,34–36,39,41–49,52]. Most importantly, none of the VDU-based filter structures can operate in mixed-mode configuration.

In this research, a first-of-a-kind VDBA-based MISO type mixed-mode universal filter is proposed that can work in all four modes of operation, providing all five filter responses. The proposed structure without any change in the core topology can also function as a SIMO filter providing CM output. The validation of the VDBA and filter is carried out in Cadence design software using 0.18 μm Silterra Malaysia PDK. Both simulation and experimental results are in close agreement with the theoretical findings.

Table 1. Comparative study of various VDU-based SIMO-type biquad filter designs with the proposed filter (Note: NA—not applicable).

References	(i)	(ii)	(iii)	(iv)	(v)	(vi)	(vii)	(viii)	(ix)	(x)	(xi) (MHz)	(xii) (W)	(xiii) (V)	(xiv)
[25]	2-FB-VDBA	2C + 4R	Yes	NA	NA	Yes	NA	VM/CM	No	No	1	–	±5	–
[28]	2-FB-VDIBA	2C + 4R	Yes	NA	NA	Yes	NA	VM	No	No	7.9	476 μ	±0.4	–
[29]	2-VD-DIBA	2C	No	NA	NA	No	NA	VM	No	No	0.159	–	±5	0.76% @ 1.07 V (for HP VM mode)
[33]	1-ZC-VDBA	2C	No	NA	NA	NA	No	CM	No	No	10	–	±0.9	≤10% @ 25 μA (for LP VM mode)
[38]	1-VDBA	2C + 3R	No	NA	NA	Yes	NA	VM	No	No	1.59	–	±0.9	–
[39]	1-VDBA	2C + 2R	No	NA	NA	NA	No	CM	No	Yes	0.78	–	±1.2	–
[40]	3-VDBA	2C	No	NA	NA	Yes	NA	VM	No	No	0.0469	–	±2	–
[53]	2-VD-DIBA	2C + 2R	No	NA	NA	No	NA	VM	Yes	No	0.1	–	±0.9	≥1.8% @ 400 mV (for LP VM mode)
This work	3-VDBA	2C	No	NA	NA	NA	Yes except (HP)	CM/TAM	Yes	Yes	16.32	5.482 m	±1.25	≤4% @ 300 mV (for HP VM mode)

Table 2. Comparative study of various VDU-based MISO-type biquad filter designs with the proposed filter (Note: NA—not applicable).

References	(i)	(ii)	(iii)	(iv)	(v)	(vi)	(vii)	(viii)	(ix)	(x)	(xi) (MHz)	(xii) (W)	(xiii) (V)	(xiv)
[23]	2-VDBA	2C	No	Yes	No	Yes	NA	VM	No	Yes	1.19	970 μ	±1.5	≤1% @ 0.4 V (for BP VM mode)
[26]	1-VDIBA	2C + R	No	No	NA	No	NA	VM	No	Yes	1.34	–	–	–
[30]	2-VDBA	2C	No	No	NA	Yes	NA	VM	No	No	0.1	–	±0.2	>1.5% @ 50 mV (for VM mode)
[31]	2-VDIBA	2C	No	No	NA	No	NA	VM	Yes	No	2.06	–	±0.4	–
[32]	1-VDBA	2C + 2R	Yes	No	No	No	NA	VM	No	No	0.88	–	±0.9	–
[34]	2-VDIBA	2C	No	No	NA	Yes	NA	VM	No	Yes	12.9	2.8 m	±0.75	≤1% @ 85 mV (for VM mode)
[35]	2-VDIBA	2C + R	No	Yes	No	Yes	NA	VM	Yes	Yes	10.1	1.14 m	±0.6	0.4% @ 25 mV (for VM mode)
[36]	2-VDBA	2C	No	No	No	Yes	NA	VM	No	Yes	56	440.6 n	±0.7	–
[37]	2-VDBA	2C	No	No	No	Yes	NA	VM	No	No	47	–	–	–
[41]	1-VD-DIBA	2C + R	Yes	No	Yes	Yes	NA	VM	No	Yes	–	–	±2	–
[42]	1-VDIBA	2C	No	No	No	No	NA	VM	No	Yes	1.59	–	±0.9	3.15% @ 50 mV (for BP VM mode)
[43]	1-VDBA	2C	No	No	No	Yes	NA	VM	No	Yes	0.766	–	–	–
[44]	2-VDBA	2C	No	Yes	No	Yes	NA	VM	No	Yes	1.16	–	±1.5	>3.15% @ 0.8 V (for BP VM mode)
[45]	2-VDBA	2C	No	Yes	No	Yes	NA	VM	No	Yes	10.16	–	±1.5	≤4% @ 28 mV (for VM mode)

Table 2. *Cont.*

References	(i)	(ii)	(iii)	(iv)	(v)	(vi)	(vii)	(viii)	(ix)	(x)	(xi) (MHz)	(xii) (W)	(xiii) (V)	(xiv)
[46]	2-VD-DIBA	2C	No	No	Yes	Yes	NA	VM	No	Yes	0.1563	–	±5	–
[47]	2-VDBA	2C	No	Yes	No	Yes	NA	VM	No	Yes	22	750 μ	±0.75	≥2% @ 50 mV (for BP VM mode)
[48]	1-VDBA	2C + R	No	Yes	No	No	NA	VM	No	Yes	–	–	±1.5	–
[49]	1-VDBA	2C + R	No	Yes	No	No	NA	VM	Yes	Yes	19.49	360 μ	±0.75	–
[50]	2-VDIBA	2C + R	No	No	No	No	NA	VM	Yes	No	–	–	±0.6	–
[51]	2-VD-DIBA	2C + 2R	No	No	No	No	NA	VM	Yes	No	0.3093	–	±5	>4% @ 90 mV (for BP VM mode)
[52]	2-VDBA	2C	No	Yes	No	Yes	NA	VM	No	Yes	0.05	–	±5	2.98% @ 50 mV (for BP VM mode)
[53]	2-VD-DIBA	2C + 2R	Yes	No	No	Yes	NA	VM	Yes	Yes	0.1	–	–	–
[54]	3-VDBA	2C + 2R	No	No	No	Yes	Yes	VM, TAM	Yes	Yes	7.2	5.47 m	±1.25	≤6% @ 250 mV (for BP VM mode)
This work	3-VDBA	2C + R	No	No	No	Yes	Yes	VM, CM, TIM, TAM	Yes	Yes	16.34	5.482 m	±1.25	≤4% @ 350 mV (for HP VM mode)

2. Voltage Differencing Buffered Amplifier (VDBA)

The VDBA simply is a cascade connection of a voltage buffer and an operational transconductance amplifier (OTA). The voltage-current relationship of the VDBA is presented in Equation (1) and the functional block representation is given in Figure 1a.
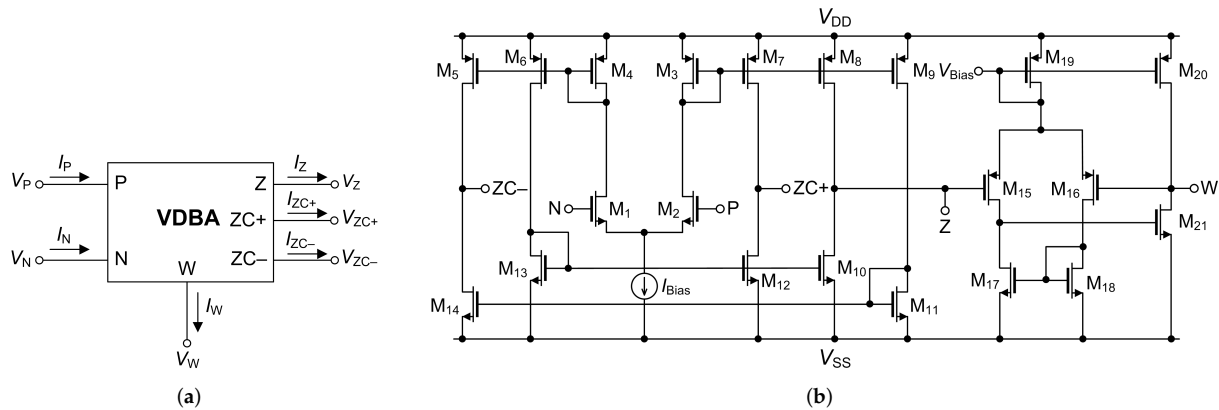

Figure 1. (**a**) Block diagram and (**b**) CMOS implementation of VDBA.

$$
\begin{bmatrix} I_P \\ I_N \\ I_Z \\ I_{ZC+} \\ I_{ZC-} \\ V_W \end{bmatrix} = \begin{bmatrix} 0 & 0 & 0 \\ 0 & 0 & 0 \\ g_m & -g_m & 0 \\ g_m & -g_m & 0 \\ -g_m & g_m & 0 \\ 0 & 0 & 1 \end{bmatrix} \begin{bmatrix} V_P \\ V_N \\ V_Z \end{bmatrix}.
\tag{1}
$$

The VDBA is a six-terminal device, of which CMOS implementation is shown in Figure 1b. The first transconductance amplifier stage is built by the transistors M1–M14. The output current of the transconductance amplifier depends on the difference in voltage between P and N terminals. If operation in saturation region is assumed and W/L ratio for transistors M1 and M2 are made identical then the output current I_Z of the OTA is given by Equation (2): The voltage follower forms the second stage of the VDBA designed using transistors M15–M21.

$$
I_Z = g_m(V_P - V_N) = \left(\sqrt{2I_{Bias}K_i} \right)(V_P - V_N),
\tag{2}
$$

where the transconductance parameter $K_i = \mu C_{ox} W/2L$ $(i = 1, 2)$, W is the effective channel width, L is the effective length of the channel, C_{ox} is the gate oxide capacitance per unit area, and μ is the carrier mobility.

3. Proposed Universal Filter

The proposed filter shown in Figure 2 utilizes three VDBAs and three passive components. The filter provides all five filter responses in all four modes of operation in MISO configuration. The filter can also be used in SIMO configuration wherein it provides CM responses. The MISO filter has the following features: (i) ability to operate in all four modes of operation, (ii) low output impedance for VM/TIM and high input impedance for CM/TAM, (iii) no passive component matching required, (iv) no need for inverting inputs for response realization, and (v) inbuilt tunability of quality factor independent of pole frequency.
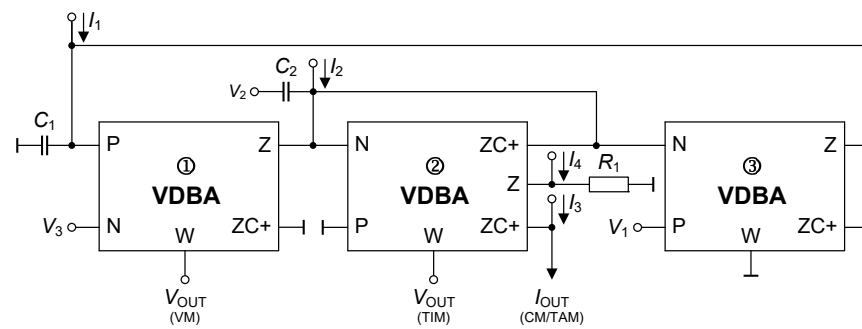
Figure 2. Proposed MISO mixed-mode universal filter.

3.1. Operation in VM and TAM Modes

In VM, the input voltage (V_{IN}) is applied according to Table 3 to obtain all five filter responses, namely LP, BP, HP, BR, and AP. Equations (3) and (4) give the transfer function of the VM and TAM, while Equations (5) and (6) give the expression for the characteristic frequency and quality factor. The input current (I_{IN}) is set to zero.

$$V_{OUT(VM)} = \frac{s^2 C_1 C_2 V_2 - s C_1 g_{m1} V_3 + g_{m1} g_{m3} V_1}{s^2 C_1 C_2 + s C_1 g_{m2} + g_{m1} g_{m3}}, \tag{3}$$

$$I_{OUT(TAM)} = -g_{m2} \left[\frac{s^2 C_1 C_2 V_2 - s C_1 g_{m1} V_3 + g_{m1} g_{m3} V_1}{s^2 C_1 C_2 + s C_1 g_{m2} + g_{m1} g_{m3}} \right], \tag{4}$$

$$\omega_0 = \sqrt{\frac{g_{m1} g_{m3}}{C_1 C_2}}, \tag{5}$$

$$Q = \frac{1}{g_{m2}} \sqrt{\frac{g_{m1} g_{m3} C_2}{C_1}}. \tag{6}$$

Table 3. Input voltage excitation sequence.

Response	Inputs		
	V_1	V_2	V_3
LP	V_{in}	0	0
HP	0	V_{in}	0
BP	0	0	V_{in}
BR	V_{in}	V_{in}	0
AP	V_{in}	V_{in}	V_{in}

3.2. Operation in Current- and Trans-Impedance-Modes

In CM mode, the input voltage (V_{IN}) is set to zero and input currents are applied according to Table 4 to obtain all five filter responses. Equations (7) and (8) give the transfer functions of the CM modes.

$$I_{OUT(CM)} = \frac{(s^2 C_1 C_2 + s C_1 g_{m2} + g_{m1} g_{m3}) I_3 - s C_1 g_{m2} I_2 - g_{m1} g_{m2} I_1}{s^2 C_1 C_2 + s C_1 g_{m2} + g_{m1} g_{m3}}, \tag{7}$$

$$V_{OUT(TIM)} = R_1 \left[\frac{(s^2 C_1 C_2 + s C_1 g_{m2} + g_{m1} g_{m3}) I_4 - s C_1 g_{m2} I_2 - g_{m1} g_{m2} I_1}{s^2 C_1 C_2 + s C_1 g_{m2} + g_{m1} g_{m3}} \right]. \tag{8}$$

In the current- and trans-impedance-modes of operation, only three input currents will be used. For CM, currents I_1, I_2, I_3 and for TIM currents I_1, I_2, I_4 will be applied, respectively. In addition, to realize AP response I_2 with double magnitude is required. It can be easily generated by applying two currents of equal magnitude at the input node

without requiring any additional hardware. Furthermore, the gain of the TIM response can be adjusted using the resistor R_1.

Table 4. Input current excitation sequence.

Response	Inputs			
	I_1	I_2	I_3	I_4
LP	I_{in}	0	0	0
HP	I_{in}	I_{in}	I_{in}	I_{in}
BP	0	I_{in}	0	0
BR	0	I_{in}	I_{in}	I_{in}
AP	I_{in}	$2I_{in}$	I_{in}	I_{in}

3.3. SIMO Filter Configuration

Figure 3 shows the SIMO filter topology. It can be seen from the figure that the core circuit remain unchanged and the resistor R_1 is no longer required leading to resistorless implementation. The only drawback is the availability of the HP output through the capacitor. The HP current can be sensed using a current follower. In the SIMO configuration, the filter can function in CM mode by providing all five filter responses.
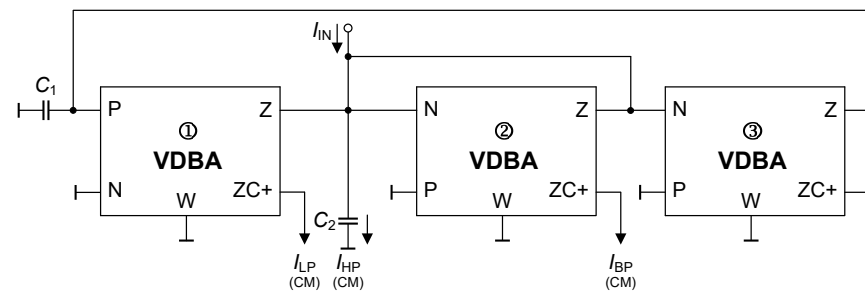

Figure 3. Proposed SIMO dual-mode universal filter.

For the current-mode of operation, V_{IN} is set to zero and current I_{IN} is applied to the filter topology. The transfer functions in the CM are given in Equations (9)–(13), while a corresponding quality factor and pole frequency are given in Equations (14) and (15).

$$\frac{I_{LP}}{I_{IN}} = \frac{g_{m1}g_{m3}}{s^2 C_1 C_2 + s C_1 g_{m2} + g_{m2}g_{m3}}, \tag{9}$$

$$\frac{I_{HP}}{I_{IN}} = \frac{s^2 C_1 C_2}{s^2 C_1 C_2 + s C_1 g_{m2} + g_{m2}g_{m3}}, \tag{10}$$

$$\frac{I_{BP}}{I_{IN}} = \frac{-s C_1 g_{m2}}{s^2 C_1 C_2 + s C_1 g_{m2} + g_{m2}g_{m3}}. \tag{11}$$

$$\frac{I_{BR}}{I_{IN}} = \frac{g_{m1}g_{m3} + s^2 C_1 C_2}{s^2 C_1 C_2 + s C_1 g_{m2} + g_{m2}g_{m3}}, \tag{12}$$

$$\frac{I_{AP}}{I_{IN}} = \frac{g_{m1}g_{m3} - s C_1 g_{m2} + s^2 C_1 C_2}{s^2 C_1 C_2 + s C_1 g_{m2} + g_{m2}g_{m3}}, \tag{13}$$

$$\omega_0 = \sqrt{\frac{g_{m2}g_{m3}}{C_1 C_2}}, \tag{14}$$

$$Q = \sqrt{\frac{g_{m3}C_2}{g_{m2}C_1}}. \tag{15}$$

Note that the BR and AP responses can be obtained by summing the LP, HP, and BP currents, $I_{\text{BR}} = I_{\text{LP}} + I_{\text{HP}}$ and $I_{\text{AP}} = I_{\text{LP}} + I_{\text{HP}} + I_{\text{BP}}$.

4. Non-Ideal Analysis

The mismatch between current mirrors, process variation and the device mismatch between the MOS transistors results in variation in the frequency dependent voltage and current transfer gains of the VDBA. This change in the gain from the ideal value of unity results in the deviation in the center frequency and quality factor of the filter. The effect of frequency dependent non-deal voltage and current transfer gains is analyzed in this section. The (β) denotes the frequency dependent non-ideal voltage transfer gain and (γ) represents the transconductance transfer gain of the OTA. Considering the effect of the non-ideal gains the V-I characteristics of the VDBA will be modified as given in Equations (16)–(18), where $\beta_m = 1 - \epsilon_{vm}$ and $\gamma_m = 1 - \epsilon_{gm}$, for $m = 1, 2$, which refers to the number of VDBAs. Here, $\epsilon_{vm}(|\epsilon_{vm}| \ll 1)$ denote voltage tracking error, and $\epsilon_{gm}(|\epsilon_{gm}| \ll 1)$ denote transconductance errors of the VDBA.

The modified transfer function and expressions for center frequency and quality factor including the non-ideal effect is given in Equations (19)–(24) for the MISO filter. The non-idealities result in deviations from the expected value.

$$I_Z = I_{\text{ZC+}} = \gamma g_{\text{m}}(V_P - V_N), \tag{16}$$

$$I_{\text{ZC-}} = \gamma' g_{\text{m}}(V_P - V_N), \tag{17}$$

$$V_Z = \beta_{\text{m}} V_W. \tag{18}$$

$$V_{\text{OUT(VM)}} = \beta_1 \left[\frac{s^2 C_1 C_2 V_2 - s C_1 g_{\text{m1}} \gamma_1 V_3 + g_{\text{m1}} g_{\text{m3}} \gamma_1 \gamma_3 V_1}{s^2 C_1 C_2 + s C_1 g_{\text{m2}} + \gamma_1 \gamma_3 g_{\text{m1}} g_{\text{m3}}} \right], \tag{19}$$

$$I_{\text{OUT(CM)}} = \left[\frac{(s^2 C_1 C_2 + s C_1 g_{\text{m2}} + \gamma_1 \gamma_3 g_{\text{m1}} g_{\text{m3}}) I_3 - s C_1 g_{\text{m2}} \gamma_2 \beta_1 I_2 - \gamma_1 \gamma_2 \beta_1 g_{\text{m1}} g_{\text{m2}} I_1}{s^2 C_1 C_2 + s C_1 g_{\text{m2}} + \gamma_1 \gamma_3 g_{\text{m1}} g_{\text{m3}}} \right], \tag{20}$$

$$I_{\text{OUT(TAM)}} = -\gamma_2 \beta_1 g_{\text{m2}} \left[\frac{s^2 C_1 C_2 V_2 - s C_1 g_{\text{m1}} \gamma_1 V_3 + g_{\text{m1}} g_{\text{m3}} \gamma_1 \gamma_3 V_1}{s^2 C_1 C_2 + s C_1 g_{\text{m2}} + \gamma_1 \gamma_3 g_1 g_{\text{m3}}} \right], \tag{21}$$

$$V_{\text{OUT(TIM)}} = R_1 \left[\frac{(s^2 C_1 C_2 + s C_1 g_{\text{m2}} + \gamma_1 \gamma_3 g_{\text{m1}} g_{\text{m3}}) I_4 - s C_1 g_{\text{m2}} \gamma_2 \beta_1 I_2 - \gamma_1 \gamma_2 \beta_1 g_{\text{m1}} g_{\text{m2}} I_1}{s^2 C_1 C_2 + s C_1 g_{\text{m2}} + \gamma_1 \gamma_3 g_{\text{m1}} g_{\text{m3}}} \right], \tag{22}$$

$$\omega_0 = \sqrt{\frac{\gamma_1 \gamma_3 g_{\text{m1}} g_{\text{m3}}}{C_1 C_2}}, \tag{23}$$

$$Q = \frac{1}{g_{\text{m2}}} \sqrt{\frac{\gamma_1 \gamma_3 g_{\text{m1}} g_{\text{m3}} C_2}{C_1}}. \tag{24}$$

The non-ideal expressions of the filter transfer function for the CM SIMO filter are given as follows:

$$\frac{I_{\text{LP}}}{I_{\text{IN}}} = \frac{\gamma_1 \gamma_3 g_{\text{m1}} g_{\text{m3}}}{s^2 C_1 C_2 + s C_1 g_{\text{m2}} + \gamma_1 \gamma_3 g_{\text{m1}} g_{\text{m3}}}, \tag{25}$$

$$\frac{I_{\text{HP}}}{I_{\text{IN}}} = \frac{s^2 C_1 C_2}{s^2 C_1 C_2 + s C_1 g_{\text{m2}} + \gamma_1 \gamma_3 g_{\text{m1}} g_{\text{m3}}}, \tag{26}$$

$$\frac{I_{\text{BP}}}{I_{\text{IN}}} = \frac{-s C_1 g_{\text{m2}} \gamma_2}{s^2 C_1 C_2 + s C_1 g_{\text{m2}} + \gamma_1 \gamma_3 g_{\text{m1}} g_{\text{m3}}}. \tag{27}$$

The sensitivities of ω_0 and Q with respect to the non-ideal gain and passive elements are calculated. Equations (28)–(30) indicate identical sensitivities for the MISO mixed-mode universal filter and CM SIMO filter.

$$-S_{C_1}^{\omega_0} = -S_{C_2}^{\omega_0} = S_{\gamma_1}^{\omega_0} = S_{\gamma_3}^{\omega_0} = S_{g_{m1}}^{\omega_0} = S_{g_{m3}}^{\omega_0} = \frac{1}{2}, \tag{28}$$

$$-S_{C_1}^{Q} = S_{g_{m1}}^{Q} = S_{g_{m3}}^{Q} = S_{C_2}^{Q} = S_{\gamma_1}^{Q} = S_{\gamma_3}^{Q} = \frac{1}{2}, \tag{29}$$

$$-S_{g_{m2}}^{Q} = 1. \tag{30}$$

The sensitivities are not greater than one, which is desired.

5. Parasitic Analysis

The block diagram presented in Figure 4 shows the various parasitic impedance associated with different terminals of the VDBA. The parasitic resistances and capacitance appear in parallel with the P, N, and Z terminals. The low impedance W terminal has a resistance in series with the inductance. For the frequency of interest, the inductance effect can be ignored. The denominator of the filter transfer function is modified in the presence of the parasitic effect as given in Equation (31).

$$D'(s) \cong s^2 C_1' C_2' + s C_1' g_{m2} + s C_2' R_A' + g_{m2} R_A' + g_{m1} g_{m3} + R_B s C_1' + R_B R_A' \tag{31}$$

where $R_A' \cong R_{P1} || R_{Z3}$, $R_1' \cong R_1 || R_{Z2}$, $R_B \cong R_{N2} || R_{Z1} || R_{Z2}$, $C_1' \cong C_1 + C_{P1} + C_{Z3}$ and $C_2' \cong C_2 + s C_{N2} + C_{Z1} + C_{Z2}$.

$$V_{OUT(VM)}' \cong \frac{(s^2 C_1' C_2' + R_A') V_2 - (s C_1' + R_A') g_{m1} V_3 + g_{m1} g_{m3} V_1}{s^2 C_1' C_2' + C_1' g_{m2} + s C_2' R_A' + g_{m2} R_A' + g_{m1} g_{m3} + R_B s C_1' + R_B R_A'} \tag{32}$$

$$I_{OUT(CM)}' \cong \frac{(s^2 C_1' C_2' + s C_1' g_{m2} + s C_2' R_A' + g_{m2} R_A' + g_{m1} g_{m3}) I_3 - (s C_1' + R_A') g_{m2} I_2 - g_{m1} g_{m2} I_1}{s^2 C_1' C_2' + s C_1' g_{m2} + s C_2' R_A' + g_{m2} R_A' + g_{m1} g_{m3} + R_B s C_1' + R_B R_A'} \tag{33}$$

$$Q' \cong \sqrt{\frac{g_{m2} R_A' + g_{m1} g_{m3} + R_B R_A'}{C_1' C_2'} \times \left(\frac{C_1' C_2'}{C_1' g_{m2} + C_2' R_A' + R_B C_1'} \right)^2} \tag{34}$$

$$\omega_0' \cong \sqrt{\frac{g_{m2} R_A' + g_{m1} g_{m3} + R_B R_A'}{C_1' C_2'}} \tag{35}$$

If R_{P1} and R_{Z3} are made greater, the $R_A' \cong 0$ the expression for Q' and ω_0' will be simplified as given below.

$$Q' \cong \frac{1}{g_{m2} + R_B} \sqrt{\frac{C_2' (g_{m1} g_{m3})}{C_1'}} \tag{36}$$

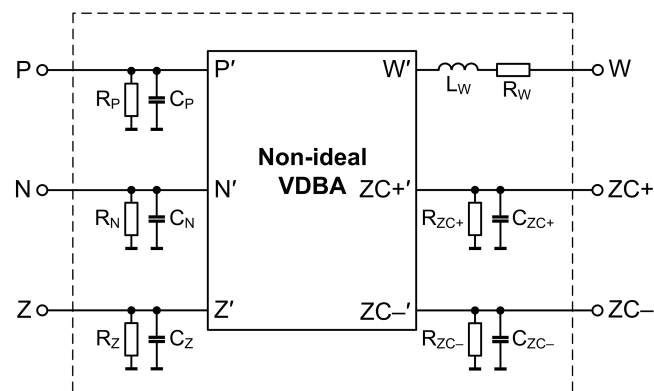$$\omega_0' \cong \sqrt{\frac{g_{m1} g_{m3}}{C_1' C_2'}} \tag{37}$$

Figure 4. Non-ideal model of VDBA.

6. Simulation Results

To validate the performance of the designed VDBA-based mixed-mode universal filter, it was designed and simulated in Silterra Malaysia 0.18 μm technology using Cadence Virtuoso software. The supply voltages ±1.25 V are used. The width and length of the MOS transistors in Figure 1b are given in Table 5, while the design metrics of the VDBA active block are listed in Table 6.

Table 5. Width and length of the MOS transistors.

Transistor	Width (μm)	Length (μm)
M1–M4, M10–M16	1.8	0.36
M5–M9	5.4	0.36
M17–M18	1.2	0.36
M19–M20	4.8	0.36
M21	2.4	0.36

Table 6. Performance metrics of the VDBA.

Parameters	Values
Parasitics at nodes P and N @ 1 kHz: $R_P = R_N$	25 GΩ
Parasitics at W node: R_W, L_W	140.89 Ω, 0.923 μH
Parasitics at nodes Z, ZC+, ZC−: $R_Z = R_{ZC+} = R_{ZC-}$, $C_Z = C_{ZC+} = C_{ZC-}$	64.4 kΩ, 26.3 fF
Voltage gain: V_W / V_Z	0.985
Voltage transfer bandwidth: V_W / V_Z	3.0262 GHz
DC voltage range: $V_Z - V_W$	±900 mV
Static power dissipation	1.618 mW

The developed filter is designed for a pole frequency of 16.631 MHz by selecting component values as $C_1 = C_2 = 10$ pF, $R_1 = 1$ kΩ, and $g_{m(1-3)} = 1.045$ mA/V. It must be mentioned that results provided for the filter are pre-layout results considering the nominal values as provided in the Silerra Malaysia PDK. The proposed filter is suitable for wide variety of applications in industrial signal processing and wireless communication, etc. The frequency-domain responses of the filter in all four modes are presented in Figures 5–8. To test the quality factor tuning independent of the frequency BP response is plotted for different values of the bias current I_{Bias1}. It can be inferred from Figure 9 that the quality factor can be tuned without disturbing the frequency.
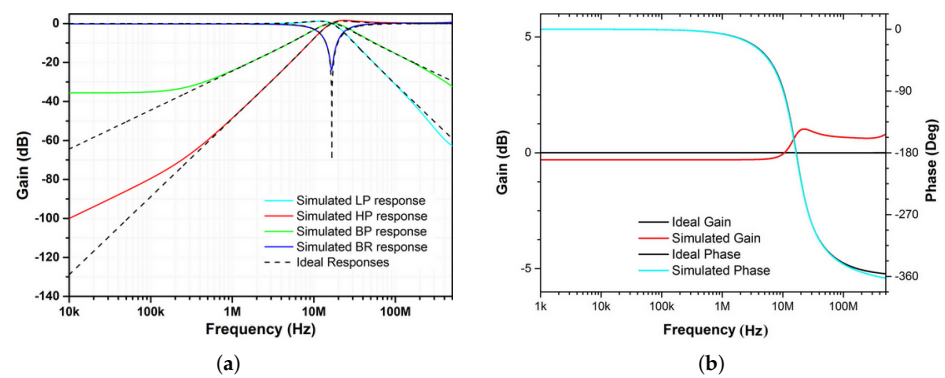
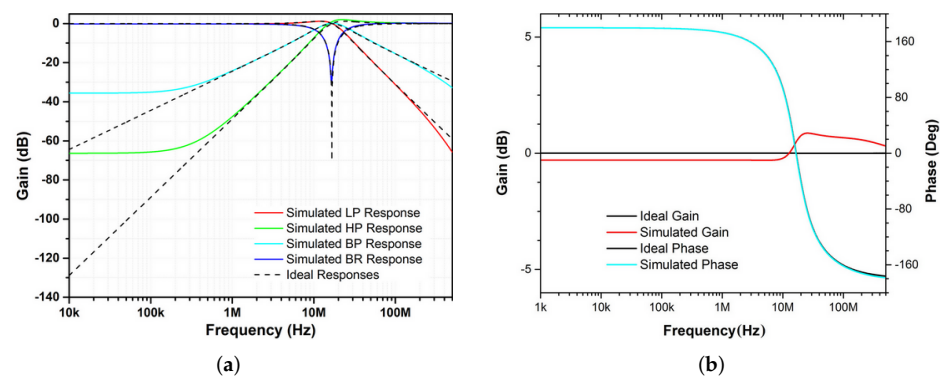**Figure 5.** Frequency response of the MISO VM Filter: (**a**) LP, BP, HP, and BR (**b**) AP.

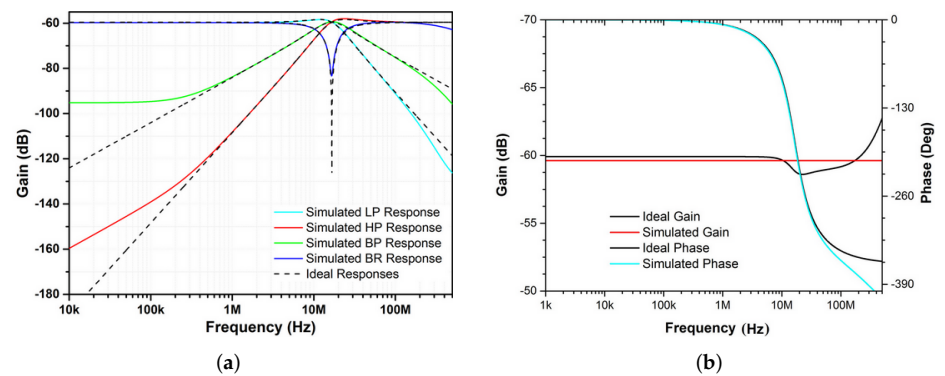**Figure 6.** Frequency response of the MISO CM Filter: (**a**) LP, BP, HP, and BR (**b**) AP.

Figure 7. Frequency response of the MISO TAM Filter: (**a**) LP, BP, HP, and BR (**b**) AP.
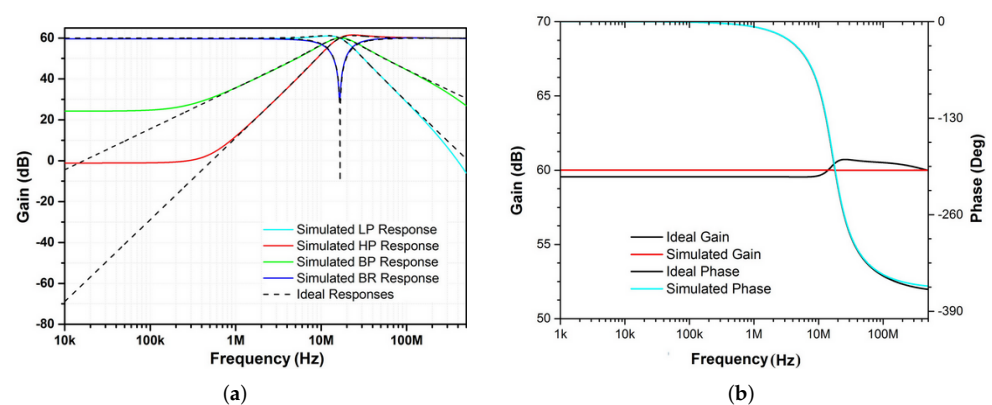

Figure 8. Frequency response of the MISO TIM Filter: (**a**) LP, BP, HP, and BR (**b**) AP.

As the OTA offset current can cause frequency and phase deviation in the designed filter, Monte Carlo analysis is carried out for 200 runs to obtain an accurate measure of the offset current at the (Z, ZC+) terminals of the OTA. The I_{Bias} of OTA is set at 120 µA. The results show minimum offset current = 1.08 µA, maximum offset current = 18.131 µA, mean offset current = 10.87 µA and standard deviation = 4.20 µA. To verify the signal processing capability of the filter, transient analysis is performed for BP responses in the VM and CM mode. In VM, a sinusoidal signal of 16.6 MHz frequency and 200 mV peak-to-peak is applied at the input and the output waveform is observed as given in Figure 10a. In CM, a sinusoidal signal of 16.6 MHz frequency and 100 µA peak-to-peak is applied and the output waveform is presented in Figure 10b. It can be observed that the filter functions correctly.

To study the effect of process spread on the designed filter, Monte Carlo analysis is done for 200 runs for VM BP and CM AP configurations as presented in Figure 11a,b. It can be deduced from the figures that there is no large variation in the pole frequency of the filter due to process variations.

The THD of the proposed filter for LP, HP, and BP responses is plotted for different input signal amplitudes for VM, as shown in Figure 12a. The THD plot for CM-BP/LP is presented in Figure 12b. As per the IEEE Std 519-2014 [55] the THD of the filter remains within acceptable limits (≤5%) for a considerable input signal range. Moreover, the THD performance of the filter is at par with other reported mixed-mode filters [10,11,13–15,19].
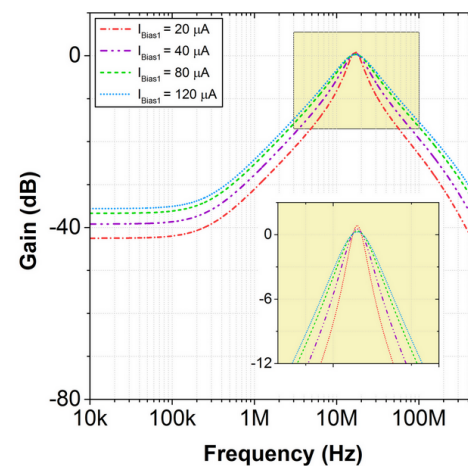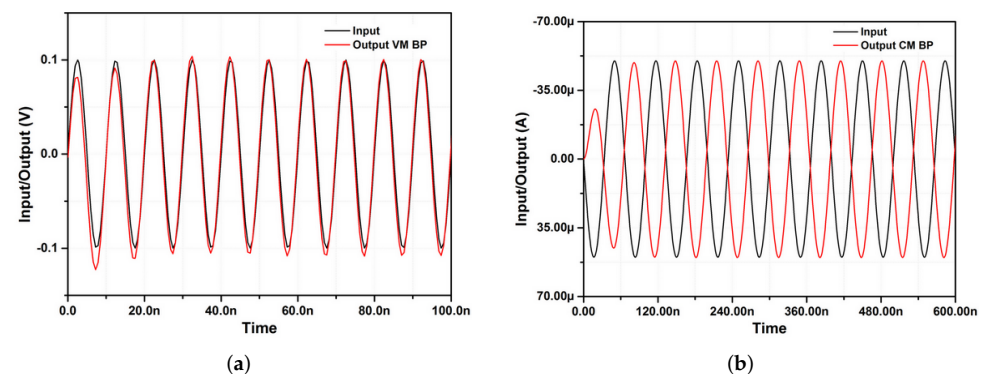

Figure 9. Quality factor tuning for CM BP filter.

(**a**)

(**b**)

Figure 10. Transient analysis result for BP filter: (**a**) VM MISO and (**b**) CM MISO configurations.
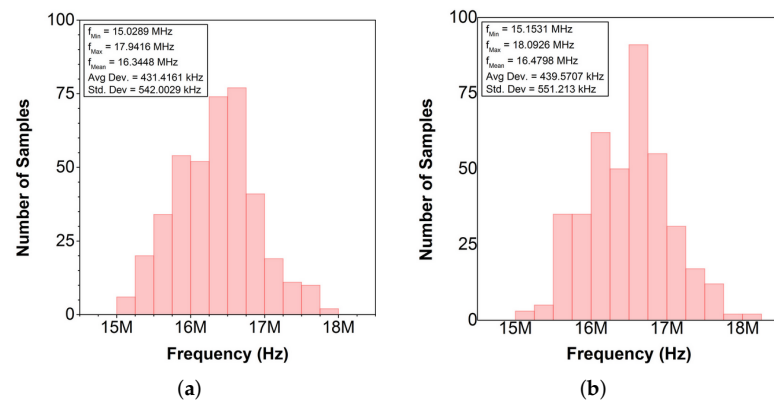
Figure 11. Monte Carlo analysis results: (**a**) BP of VM MISO, (**b**) AP of CM MISO configurations.
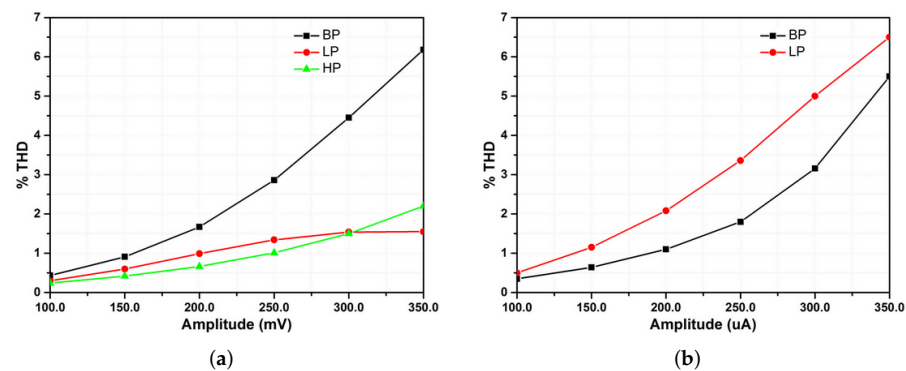

Figure 12. Total harmonic distortion results: (**a**) VM-LP, VM-HP, and VM-BP, (**b**) CM-LP and CM-BP.

The reduction in the frequency of the filter due to the increase in temperature can be ascribed to the decrease in the transconductance of the OTA. The major factors affecting the transconductance are carrier mobility (μ) and threshold voltage (V_t). The carrier mobility dependence on temperature can be modeled by Equation (38):

$$\mu_N(T) = \mu_N(T_O)\left(\frac{T}{T_O}\right)^{\alpha_\mu}, \tag{38}$$

where α_μ stands for the mobility temperature exponent, it is considered constant roughly equal to 1.5. The threshold voltage V_t can be approximated as a linear function of temperature [56,57] given by Equation (39):

$$V_t(T) = V_t(T_O) + \alpha_{V_t}(T - T_O), \tag{39}$$

here, α_{V_t} denotes the threshold voltage temperature coefficient, which varies from -1 mV/°C to -4 mV/°C and T_O is the reference temperature (300 K). These two Equations exhibit negative temperature dependence and this correlates with the decrease in the filter frequency with temperature as observed in Figure 13. The effect of noise on the performance of the proposed filter is also analyzed. The thermal and flicker noise are present in the bulk CMOS devices, and they effect the performance of the designed filter. Figure 14 gives the plot of the input and output noise for the BP VM filter configuration. At the pole frequency of the filter the input and output noises are found to be 36.2 nV/$\sqrt{\text{Hz}}$ and 36.48 nV/$\sqrt{\text{Hz}}$, respectively. It can be seen from the figure that the input and output noise are well within the acceptable limits.

To verify the CM SIMO filter, it is designed with the exact specifications of the MISO filter. The frequency responses of the filter are shown in Figure 15.

The time domain and THD analysis for the SIMO current-mode filter are presented in Figures 16 and 17. The results validate the correct functioning of the designed filter.
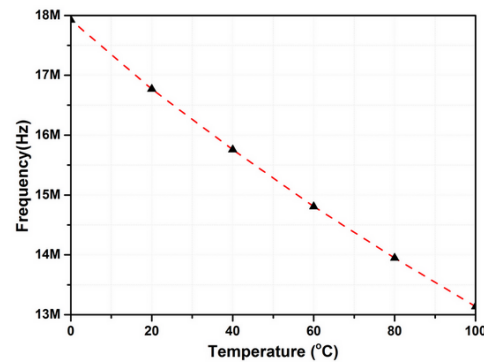

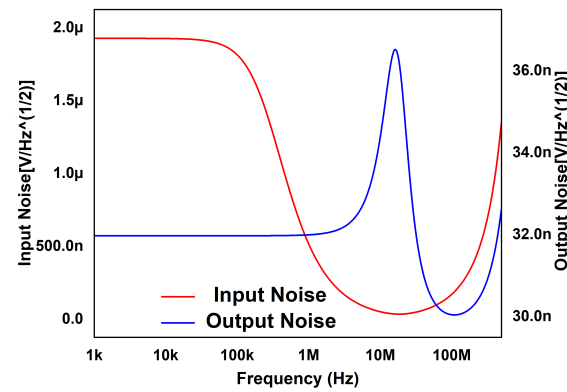**Figure 13.** CM MISO Filter: Variation of filter frequency with temperature.

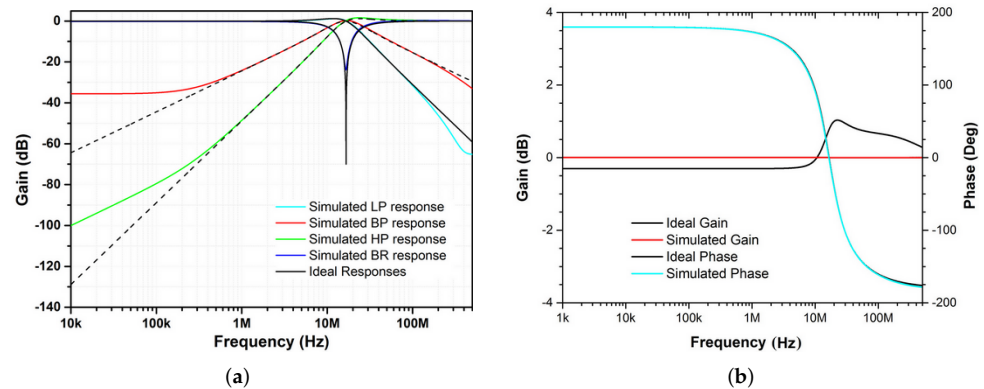**Figure 14.** Input and output noise analysis of VM BP MISO filter configuration.

(**a**)   (**b**)

Figure 15. Frequency response of the CM SIMO Filter: (**a**) LP, BP, HP, and BR filter (**b**) AP.
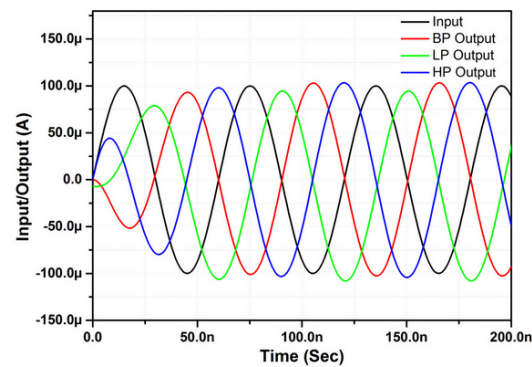
Figure 16. Transient response of the CM SIMO Filter: LP, HP, and BP.

The Monte Carlo analysis results for the designed CM BP filter response are presented in Figure 18. The frequency response and the static variations in the designed frequency are under acceptable limits.

To highlight the advantages of the designed filter, it is compared with some exemplary designs of mixed-mode filters, as shown in Table 7. By analyzing the comparison table, it can be observed that the proposed filter structure holds certain advantages over the other similar designs and also performs at par with other designs in terms of power dissipation, supply voltage, and total harmonic distortion, in addition to being the first truly mixed-mode filter based on the VDBA. The authors would like to point out that the recently reported VDBA-based mixed-mode filter designs [54,58] are not truly mixed-mode as they cannot provide all five filter responses in all four modes of operation. Furthermore, in [58] the output currents are not available from high-impedance nodes; hence extra current followers will be needed to extract the currents.
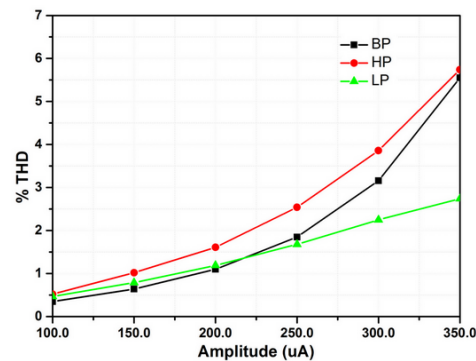

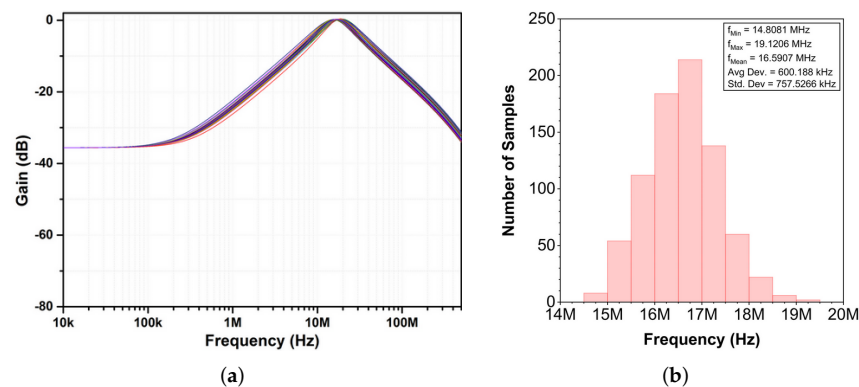**Figure 17.** Total harmonic distortion of CM SIMO filter: CM-HP, CM-LP, and CM-BP.

Figure 18. Monte Carlo analysis of CM SIMO Filter: (**a**) the results and (**b**) the corresponding histogram.

Table 7. Comparison of the proposed filter with other similar topologies.

References	No. of ABBs	No. of Passive Components	Independent Tuning of Q	All Five Filter Responses Available in Four Operation Modes	Low Output Impedance for VM and TIM	No Requirement for Double/Negative Input Signals Voltage	In-Built Tunability	Test Frequency (MHz)	Power Dissipation (W)	Supply Voltage (V)	THD
[5]/2003	6-OTA	2C	No	No	No	Yes	Yes	–	–	–	–
[6]/2004	7-CCII	2C + 8R	No	Yes	No	Yes	No	–	–	–	–
[7]/2006	3-CCII	3C + 4R + 2-switch	No	Yes	No	Yes	No	–	–	±12	–
[8]/2008	4-OTA	2C	No	No	No	Yes	Yes	2.25	–	–	–
[9]/2010	5-OTA	2C	No	Yes	No	No	Yes	1.59	–	±1.25	0.777% @ 0.4 V_{p-p} (for LP VM mode)
[10]/2010	2-MOCCCII	2C + 2R	Yes	Yes	No	Yes	Yes	1.27	–	±2.5	≤3% @ 100 μA (for BP CM mode)
[11]/2013	4-MOCCCII	2C	No	Yes	Yes	No	Yes	–	–	±1.25	≥0.5% @ 150 μA
[12]/2013	1-FDCCII	2C + 2R	No	No	No	Yes	No	10	–	±0.9	–
[13]/2013	2-VDTA	2C	Yes	No	No	Yes	Yes	1	–	±1.5	≤3% @ 400 mV (for BP VM mode)
[14]/2010	1-CFOA	2C + 3R	Yes	No	No	No	No	12.7	2.53 m	±1.25	≥4% @ 40 μA (for BP CM mode)
[15]/2016	1-FDCCII + 1-DDCC	2C + 6R	Yes	Yes	No	No	No	1.59	–	±0.9	≤4% @ 400 mV (for AP VM mode)
[16]/2018	5-DVCC	2C + 5R	Yes	Yes	No	Yes	No	1	471 μ	±0.8	–
[17]/2019	5-OTA	2C	Yes	Yes	No	Yes	Yes	3.39	191.7 μ	±0.9	–
[18]/2020	3-DDCCII	2C + 4R	No	Yes	No	Yes	No	3.978	–	±1.25	–
[19]/2016	1-MCCTA	2C + 2R	Yes	Yes	No	Yes	Yes	12.16	–	–	≤3% @ 70 μA (for BP CM mode)
[20]/2018	4-CCII	2C + 4R	Yes	No	No	Yes	No	31.8	–	–	–
This work	3-VDBA	2C + R	Yes	Yes	Yes	Yes	Yes	16.32	5.482 m	±1.25	≤4% @ 350 mV (for HP VM mode)

7. Experimental Validation

To further verify the correct functioning of the proposed filter circuit and to complement the theoretical and simulation results, detailed experimental analysis is carried out for MISO VM and TAM modes and SIMO CM configuration. The VDBA is built with available integrated circuits (ICs), the Intersil CA3080 OTAs and Texas Instruments LF356 op-amp, as shown in Figure 19. The supply voltages are set ± 5 V.
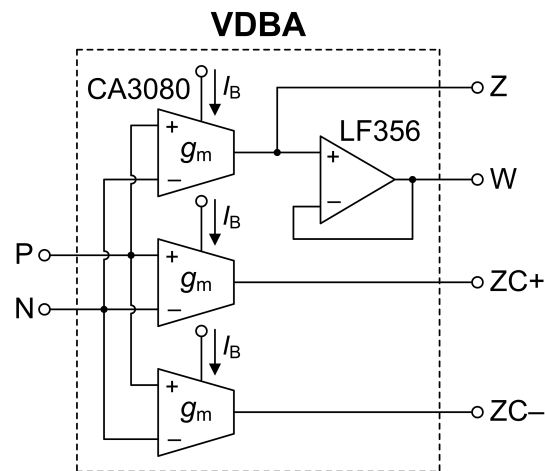

Figure 19. VDBA implementation using off-the-shelf ICs.

To design the filter for a pole frequency of $f_0 = \omega_0/2\pi = 100.27$ kHz and $Q = 1$, the active component values are selected as $g_\mathrm{m} = g_{\mathrm{m}i}$ (g_m of i-th VDBA, $i = 1, 2, 3$) = 0.63 mA/V (I_B = 31.5 μA), where $g_\mathrm{m} = \frac{I_B}{2V_T}$ and V_T is thermal voltage $\cong$ 25 mV at 27 °C. In all measurements, the passive components are chosen as $R_1 = 1$ kΩ, and $C_1 = C_2 = 1$ nF. The measured LP, HP, BP, BR, and AP frequency response results of the VM MISO configuration in Figure 2 are given in Figure 20. Figure 21 also presents the measured time-domain responses for LP, HP, BP, and BR filters, when the sinusoidal input signal of an amplitude 100 mV peak-to-peak at 100 kHz is applied. In addition, the measurement of input and output voltage waveforms of the VM AP filter and the FFT analysis results at the V_{OUT} output terminal are given in Figure 22, respectively.

For obtaining the TAM and CM SIMO filter results, two additional Analog Devices AD844s and a converting resistor (R_C) are employed to covert current to voltage. The circuit is shown in Figure 23, where the value of R_C is equal to 1 kΩ. Figure 24 shows the measured TAM filtering responses with the same component values as described above for $f_0 = 100.27$ kHz and $Q = 1$. Next, Figure 25 shows the time-domain responses of the proposed TAM operation for LP, BP, HP, and BR filters. In Figure 26, the measured input and output voltage waveforms of the TAM AP filter and its FFT spectrum analysis are, respectively, given.

In the same way, the LP, HP, and BP filter responses of the CM SIMO filter in Figure 3 are presented in Figure 27. In this case, the circuit components are the same as that used in the above design to have the following filter characteristics: $f_0 = 100.27$ kHz and $Q = 1$. As expected, the experimental results of the CM SIMO configuration are close to the theoretical results.

From the experimental results, it is evident that the proposed filter topologies are practically realizable. The deviation in the measurement results is mainly due to the breadboard circuit implementation. It is expected that, when the filter circuit is fabricated, the behavior of the proposed filter will be very close to the simulation results.
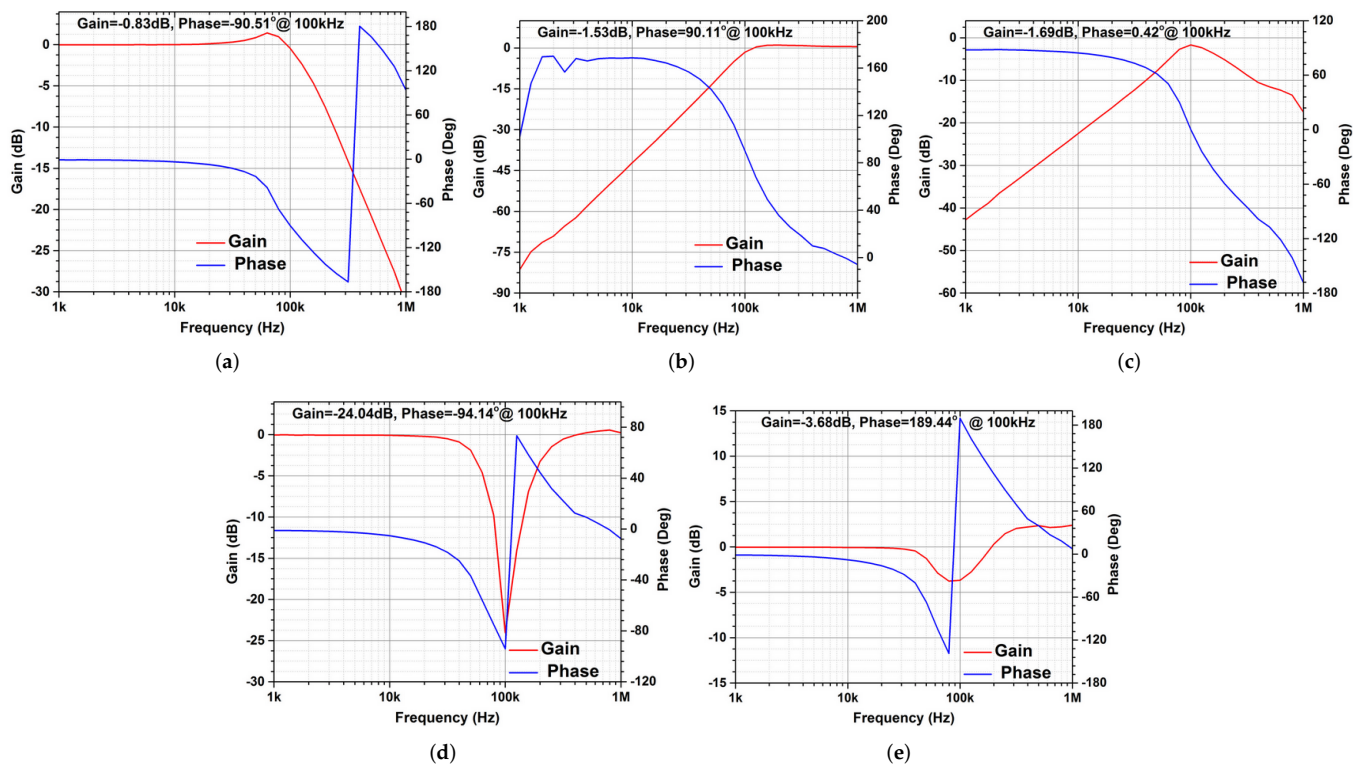
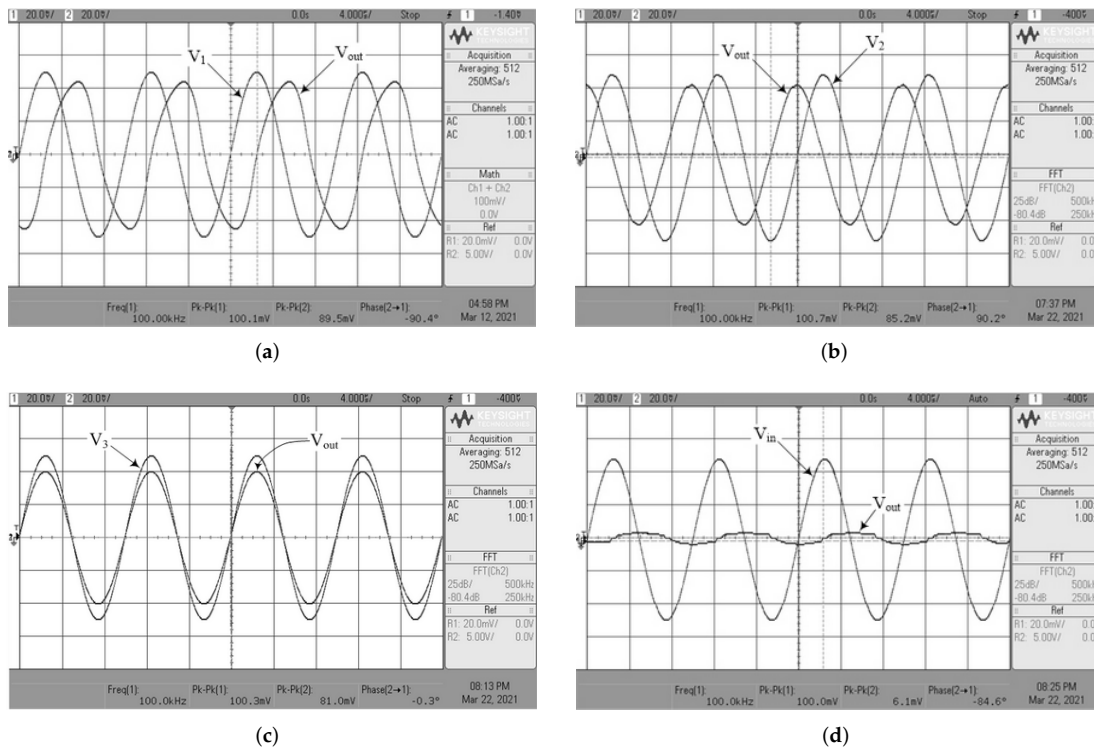**Figure 20.** VM MISO configuration: Measured gain and phase responses of the (**a**) LP, (**b**) HP, (**c**) BP, (**d**) BR, and (**e**) AP.

Figure 21. VM MISO configuration: Measured input and output waveforms of the (**a**) LP, (**b**) HP, (**c**) BP, and (**d**) BR.
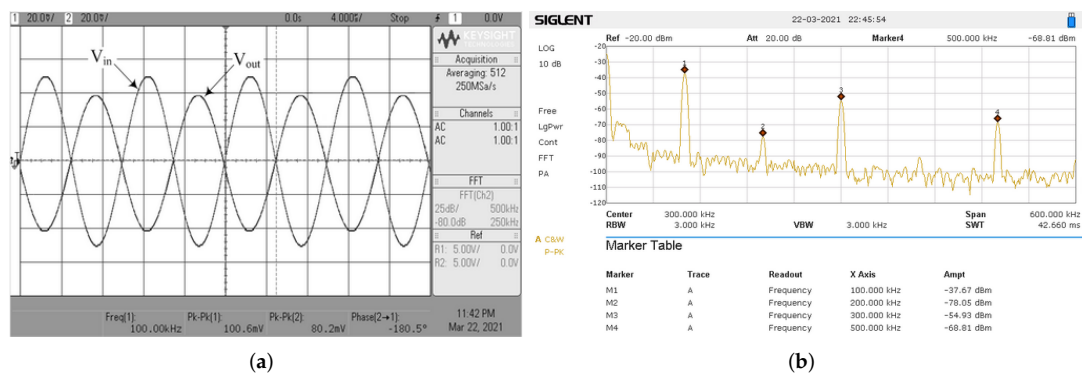
(**a**)

(**b**)

Figure 22. VM MISO configuration: (**a**) measured input and output waveforms of the AP filter, (**b**) its FFT analysis results.

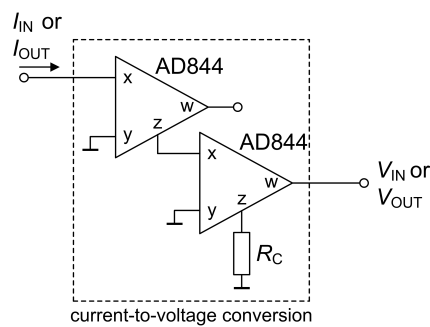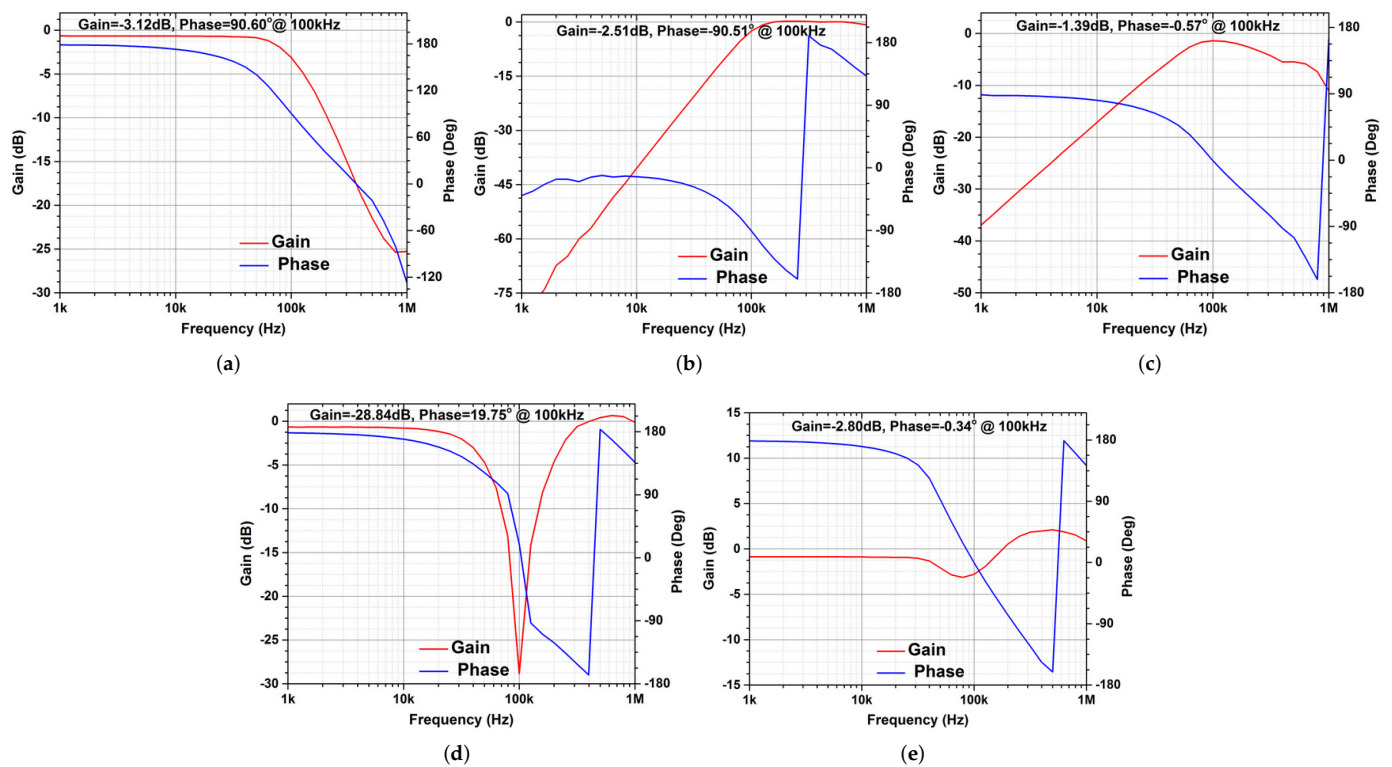**Figure 23.** Voltage to current conversion setup for obtaining TAM and CM SIMO filter results.

(**a**)

(**b**)

(**c**)

(**d**)

(**e**)

Figure 24. TAM MISO configuration: Measured gain and phase responses of the (**a**) LP, (**b**) HP, (**c**) BP, (**d**) BR, and (**e**) AP.
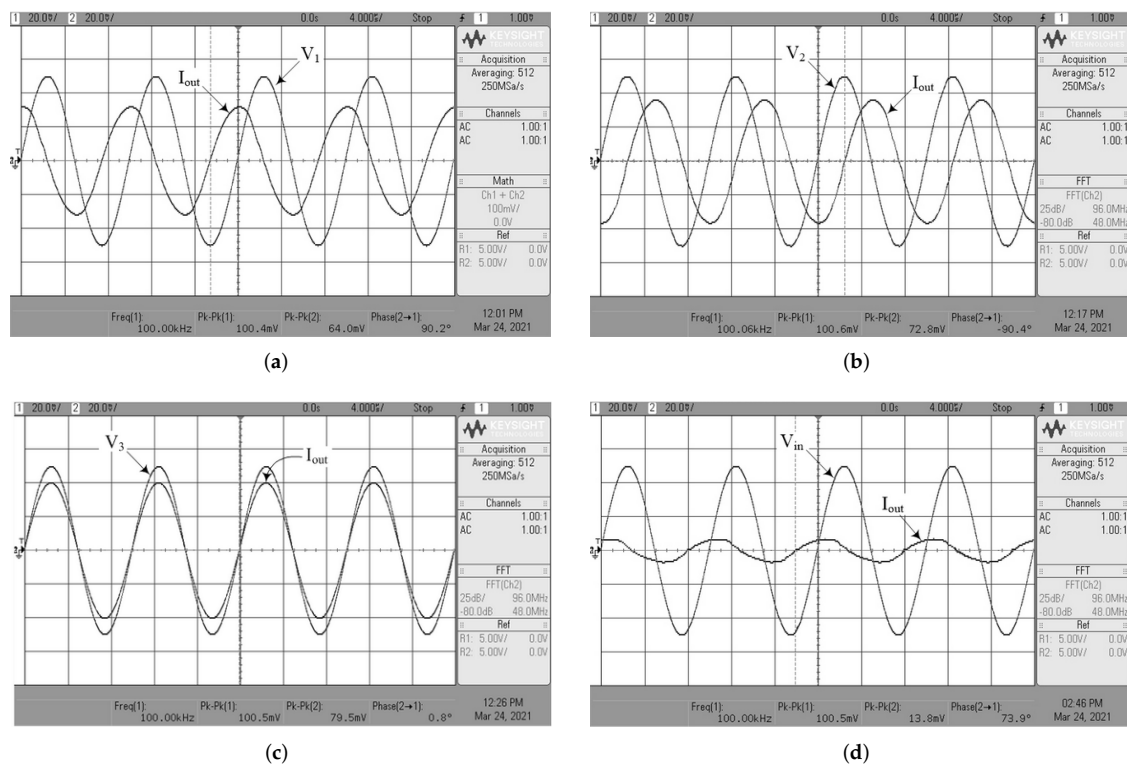
Figure 25. TAM MISO configuration: Measured input and output waveforms of the (**a**) LP, (**b**) HP, (**c**) BP, and (**d**) BR.
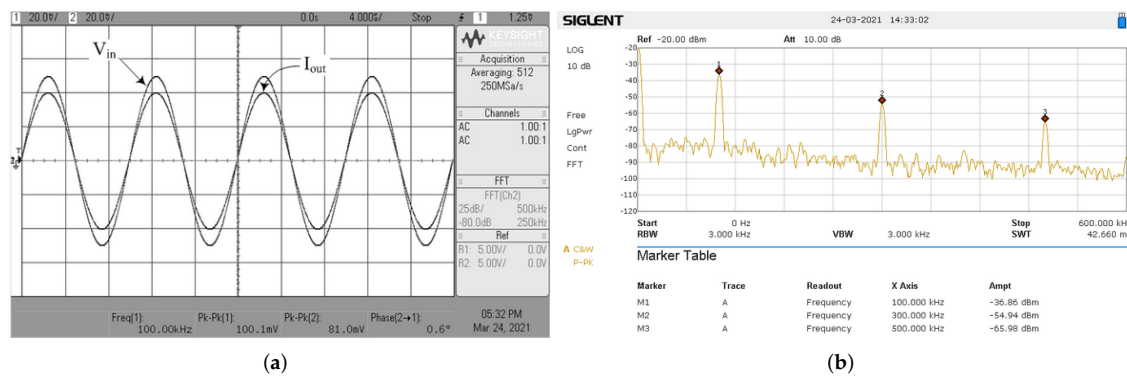

Figure 26. TAM MISO configuration: (**a**) measured input and output waveforms of the AP filter, (**b**) its FFT analysis results.
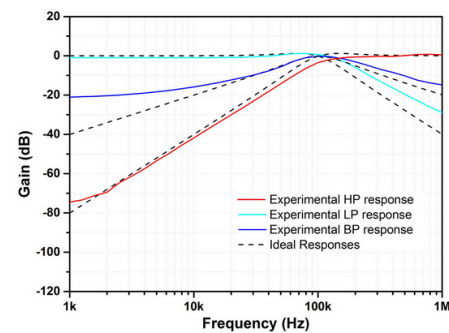

Figure 27. CM SIMO configuration: Gain responses of the LP, BP, and HP filter.

8. Conclusions

In this research, a truly mixed-mode universal filter based on VDBA is proposed. The filter requires three VDBAs, two capacitors, and a resistor for implementation. It provides all five filter responses in all four modes of operation in MISO configuration. A SIMO resistorless CM universal filter can also be derived from the same core arrangement. In MISO configuration, the VM/TIM outputs are available from low impedance nodes and CM/TAM outputs are available from high impedance node leading to cascadability. The filter has a feature of inbuilt tunability as well. The detailed theoretical analysis, non-ideal, and sensitivity analyses are performed to establish the correct functioning of the filter. The VDBA-based filter is designed and validated in Cadence Virtuoso software using Silterra Malaysia 0.18 μm PDK. The filter is designed for a characteristic frequency of 16.66 MHz with a $\pm$1.25 V supply. The Monte Carlo analysis shows that the frequency deviation is within acceptable limits. Additionally, the THD is within 5% for a substantial voltage/current input signal range. The experimental validation of the proposed filter is also carried out. The filter is constructed using commercially available ICs. The frequency responses and time-domain results of the filter confirm the correct functioning. The simulation and experimental results are found consistent with the theoretical predictions.

Abbreviations and Symbols

The following abbreviations and symbols are used in this manuscript:

β	Frequency dependent non-ideal voltage gain
γ, γ'	Frequency dependent non-ideal transconductance transfer gains
μ	Carrier mobility
ABB	Active building blocks
AP	All-pass
BP	Band-pass
BR	Band-reject
CCII	Second-generation current conveyor
CDBA	Current differencing buffer amplifier
CFOA	Current feedback operational amplifier
CM	Current-mode
C_{ox}	Gate oxide capacitance per unit area
DDCC	Differential difference current conveyor
DDCCII	Differential difference current conveyor
DVCC	Differential voltage current conveyor
EXCCTA	Extra X current conveyor transconductance amplifier
FB-VDBA	Fully balanced voltage differencing buffered amplifier
FB-VDIBA	Fully balanced voltage differencing inverting buffered amplifier
FDCCII	Fully Differential Current Conveyor

g_m	Transconductance of the operational transconductance amplifier
HP	High-pass
IC	Integrated circuit
L	Effective length of the channel
LP	Low-pass
MCCTA	Modified current conveyor trans-conductance amplifier
MISO	Multi input single output
MOCCCII	Multi output current controlled current conveyor
OTA	Operational transconductance amplifier
PDK	Process design kit
Q	Quality factor
SIMO	Single input multi output
TAM	Trans-admittance-mode
THD	Total harmonic distortion
TIM	Trans-impedance-mode
VDBA	Voltage differencing buffered amplifier
VD-DIBA	Voltage differencing differential input buffered amplifier
VDIBA	Voltage differencing inverting buffered amplifier
VDTA	Voltage differencing transconductance amplifier
VM	Voltage-mode
V_t	Threshold voltage
W	Effective channel width
ZC-VDBA	Z-copy voltage differencing buffered amplifier

References

1. Mohan, P.A. *Current-Mode VLSI Analog Filters: Design and Applications*; Springer Science & Business Media: Berlin, Germany, 2003. [CrossRef]
2. Raut, R.; Swamy, M. *Modern Analog Filter Analysis and Design: A Practical Approach*; John Wiley & Sons: Hoboken, NJ, USA, 2010. [CrossRef]
3. Biolek, D.; Senani, R.; Biolkova, V.; Kolka, Z. Active elements for analog signal processing: Classification, review, and new proposals. *Radioengineering* **2008**, *17*, 15–32.
4. Chen, H.P.; Liao, Y.Z.; Lee, W.T. Tunable mixed-mode OTA-C universal filter. *Analog Integr. Circuits Signal Process.* **2009**, *58*, 135–141. [CrossRef]
5. Abuelma'atti, M.T.; Bentrcia, A. A novel mixed-mode OTA-C filter. *Frequenz* **2003**, *57*, 157–159. [CrossRef]
6. Abuelma'atti, M.T.; Bentrcia, A.; Al-Shahrani, S.A.M. A novel mixed-mode current-conveyor-based filter. *Int. J. Electron.* **2004**, *91*, 191–197. [CrossRef]
7. Pandey, N.; Paul, S.K.; Bhattacharyya, A.; Jain, S.B. A new mixed mode biquad using reduced number of active and passive elements. *IEICE Electron. Express* **2006**, *3*, 115–121. [CrossRef]
8. Ibrahim, M.A. Design and analysis of a mixed-mode universal filter using dual-output operational transconductance amplifiers (DO-OTAs). In Proceedings of the 2008 International Conference on Computer and Communication Engineering, Kuala Lumpur, Malaysia, 13–15 May 2008; pp. 915–918. [CrossRef]
9. Lee, C.N. Multiple-Mode OTA-C Universal Biquad Filters. *Circuits Syst. Signal Process.* **2010**, *29*, 263–274. [CrossRef]
10. Pandey, N.; Paul, S.K.; Bhattacharyya, A.; Jain, S. Realization of Generalized Mixed Mode Universal Filter Using CCCIIs. *J. Act. Passiv. Electron. Devices* **2010**, *5*, 279–293.
11. Pandey, N.; Paul, S.K. Mixed mode universal filter. *J. Circuits Syst. Comput.* **2013**, *22*, 1250064. [CrossRef]
12. Kaçar, F.; Kuntman, A.; Kuntman, H. Mixed-mode biquad filter employing single active element. In Proceedings of the 2013 IEEE 4th Latin American Symposium on Circuits and Systems (LASCAS), Cusco, Peru, 27 February–1 March 2013; pp. 1–4. [CrossRef]
13. Yeşil, A.; Kaçar, F. Electronically tunable resistorless mixed mode biquad filters. *Radioengineering* **2013**, *22*, 1016–1025.
14. Yuce, E. Fully integrable mixed-mode universal biquad with specific application of the CFOA. *AEU-Int. J. Electron. Commun.* **2010**, *64*, 304–309. [CrossRef]
15. Lee, C.N. Independently tunable mixed-mode universal biquad filter with versatile input/output functions. *AEU-Int. J. Electron. Commun.* **2016**, *70*, 1006–1019. [CrossRef]
16. Tsukutani, T.; Yabuki, N. A DVCC-based mixed-mode biquadratic circuit. *J. Electr. Eng.* **2018**, *6*, 52–56. [CrossRef]
17. Bhaskar, D.R.; Raj, A.; Kumar, P. Mixed-mode universal biquad filter using OTAs. *J. Circuits Syst. Comput.* **2020**, *29*, 2050162. [CrossRef]
18. Lee, C.N.; Yang, W.C. General Mixed-Mode Single-Output DDCC-based Universal Biquad Filter. *Int. J. Eng. Res. Technol. (IJERT)* **2020**, *9*, 744–749.
19. Singh, S.V.; Tomar, R.S.; Chauhan, D.S. A new electronically tunable universal mixed-mode biquad filter. *J. Eng. Res.* **2016**, *2*, 1–21. [CrossRef]

20. Ettaghzouti, T.; Hassen, N.; Besbes, K. Novel multi-input single-output mixed-mode universal filter employing second generation current conveyor circuit. *Sens. Circuits Instrum. Syst. Ext. Pap.* **2018**, *6*, 53–64. [CrossRef]

21. Albrni, M.I.A.; Mohammad, F.; Herencsar, N.; Sampe, J.; Ali, S.H.M. Novel Electronically Tunable Biquadratic Mixed-Mode Universal Filter Capable of Operating in MISO and SIMO Configurations. *Inf. MIDEM J. Microelectron. Electron. Compon. Mater.* **2020**, *50*, 189–203. [CrossRef]

22. Tangsrirat, W. Linearly tunable voltage differencing buffered amplifier. *Rev. Roum. Des. Sci. Tech.* **2019**, *64*, 247–253.

23. Kacar, F.; Yesil, A.; Noori, A. New CMOS realization of voltage differencing buffered amplifier and its biquad filter applications. *Radioengineering* **2012**, *21*, 333–339.

24. Gupta, P.; Pandey, R. A low-power voltage differencing buffered amplifier. *Int. J. Circuit Theory Appl.* **2019**, *47*, 1402–1416. [CrossRef]

25. Biolkova, V.; Kolka, Z.; Biolek, D. Fully balanced voltage differencing buffered amplifier and its applications. In Proceedings of the 2009 52nd IEEE International Midwest Symposium on Circuits and Systems, Cancun, Mexico, 2–5 August 2009; pp. 45–48. [CrossRef]

26. Pushkar, K.L.; Bhaskar, D.R.; Prasad, D. Voltage-mode new universal biquad filter configuration using a single VDIBA. *Circuits Syst. Signal Process.* **2014**, *33*, 275–285. [CrossRef]

27. Kumari, S.; Gupta, M. New CMOS realization of high performance Voltage Differencing Inverting Buffered Amplifier and its filter application. *Analog Integr. Circuits Signal Process.* **2017**, *92*, 167–178. [CrossRef]

28. Kumari, S.; Gupta, M. A Design and Analysis of Low Voltage FB-VDIBA and Biquad Filter Application. In Proceedings of the 2018 5th International Conference on Signal Processing and Integrated Networks (SPIN), Noida, India, 22–23 February 2018; pp. 301–306. [CrossRef]

29. Jaikla, W.; Biolek, D.; Siripongdee, S.; Bajer, J. High input impedance voltage-mode biquad filter using VD-DIBAs. *Radioengineering* **2014**, *23*, 914–921.

30. Başak, M.E.; Kacar, F. Ultra-low voltage VDBA design by using PMOS DTMOS transistors. *Istanb. Univ. J. Electr. Electron. Eng.* **2017**, *17*, 3463–3469.

31. Sokmen, O.G.; Tekin, S.A.; Ercan, H.; Alci, M. A novel design of low-voltage VDIBA and filter application. *Elektron. Elektrotech.* **2016**, *22*, 51–56. [CrossRef]

32. Bansal, U.; Gupta, M.; Rai, S.K. Resistively compensated and SSF based VDBA offering high GBW and its application as a biquad filter. In Proceedings of the 2017 International Conference on Computer, Communications and Electronics (Comptelix), Jaipur, India, 1–2 July 2017; pp. 221–226. [CrossRef]

33. Güney, A.; Alaybeyoğlu, E.; Kuntman, H. New CMOS realization of Z copy voltage differencing buffered amplifier and its current-mode filter application. In Proceedings of the 2013 8th International Conference on Design & Technology of Integrated Systems in Nanoscale Era (DTIS), Abu Dhabi, UAE, 26–28 March 2013; pp. 68–71. [CrossRef]

34. Gupta, M.; Srivastava, R.; Singh, U. Low-voltage low-power FGMOS based VDIBA and its application as universal filter. *Microelectron. J.* **2015**, *46*, 125–134. [CrossRef]

35. Kumari, S.; Gupta, M. Design and Analysis of Tunable Voltage Differencing Inverting Buffered Amplifier (VDIBA) with Enhanced Performance and Its Application in Filters. *Wirel. Pers. Commun.* **2018**, *100*, 877–894. [CrossRef]

36. Srivastava, R.; Gupta, O.K.; Kumar, A.; Singh, D. Low-voltage bulk-driven self-cascode transistor based voltage differencing inverting buffered amplifier and its application as universal filter. *Microelectron. J.* **2020**, *102*, 104828. [CrossRef]

37. Mamatov, I.; Özçelep, Y.; Kaçar, F. Voltage differencing buffered amplifier based low power, high frequency and universal filters using 32 nm CNTFET technology. *Microelectron. J.* **2021**, *107*, 104948. [CrossRef]

38. Gupta, P.; Pandey, R. Single VDBA based multifunction filter. *Int. J. Control Theory Appl.* **2017**, *10*, 651–661.

39. Yadav, C.K.; Prasad, D.; Haseeb, Z.; Kumar, M. CM-Biquad filter using single DO-VDBA. *Circuits Syst.* **2018**, *9*, 133–139. [CrossRef]

40. Khatib, N.; Biolek, D. New voltage-mode universal filter based on promising structure of voltage differencing buffered amplifier. In Proceedings of the 2013 23rd International Conference Radioelektronika, Pardubice, Czech Republic, 16–17 April 2013; pp. 177–181. [CrossRef]

41. Pushkar, K.L.; Bhaskar, D.R.; Prasad, D. Voltage-mode universal biquad filter employing single voltage differencing differential input buffered amplifier. *Circuits Syst.* **2013**, *4*, 44–48. [CrossRef]

42. Herencsar, N.; Cicekoglu, O.; Sotner, R.; Koton, J.; Vrba, K. New resistorless tunable voltage-mode universal filter using single VDIBA. *Analog Integr. Circuits Signal Process.* **2013**, *76*, 251–260. [CrossRef]

43. Onjan, O.; Unhavanich, S.; Tangsrirat, W. SFG actualization of general nth-order voltage transfer functions using VDBAs. In Proceedings of the International MultiConference of Engineers and Computer Scientists, Hong Kong, China, 16–18 March 2016; pp. 585–589. [CrossRef]

44. Ismael, A.R. CMOS Implementation Of VDBA To Design Symmetric Filters. *J. Multidiscip. Eng. Sci. Technol. (JMEST)* **2016**, *3*, 4178–4181.

45. Ismael, A.R. The applications employed to design a new kind of filter using the active element (VDBA). *Kirkuk Univ. J. Sci. Stud.* **2016**, *11*. [CrossRef]

46. Ninsraku, W.; Biolek, D.; Jaikla, W.; Siripongdee, S.; Suwanjan, P. Electronically controlled high input and low output impedance voltage-mode multifunction filter with grounded capacitors. *AEU Int. J. Electron. Commun.* **2014**, *68*, 1239–1246. [CrossRef]

47. Pimpol, J.; Roongmuanpha, N.; Tangsrirat, W. Low-output-impedance electronically adjustable universal filter using voltage differencing buffered amplifiers. In Proceedings of the 8th International Conference on Informatics, Environment, Energy and Applications, Osaka, Japan, 16–19 March 2019; pp. 200–203. [CrossRef]

48. Pushkar, K.L.; Singh, G.; Kumar, S. Single VDBA-Based Voltage-Mode Universal Biquadratic Filter. In Proceedings of the 2018 2nd IEEE International Conference on Power Electronics, Intelligent Control and Energy Systems (ICPEICES), Delhi, India, 22–24 October 2018; pp. 788–791. [CrossRef]

49. Roongmuanpha, N.; Pukkalanun, T.; Tangsrirat, W. Three-Input One-Output Voltage-Mode Biquadratic Filter Using Single VDBA. In Proceedings of the 2020 8th International Electrical Engineering Congress (iEECON), Chiang Mai, Thailand, 4–6 March 2020; pp. 1–4. [CrossRef]

50. Singh, P.; Kumar, V.; Patnaik, L.P.; Islam, A. A VDIBA Based Voltage-Mode Highpass and Bandpass Filter. In *Proceedings of the Annual Convention of the Computer Society of India*; Springer Nature: Singapore, 2018; pp. 83–89. [CrossRef]

51. Jardrit, P.; Jaikla, W.; Siripogdee, S.; Chaichana, A.; Sotner, R.; Khateb, F. Design of High Input Impedance Voltage-mode Multifunction Biquad Filter with Independent Control of Natural Frequency and Quality Factor. In Proceedings of the 2020 17th International Conference on Electrical Engineering/Electronics, Computer, Telecommunications and Information Technology (ECTI-CON), Phuket, Thailand, 24–27 June 2020; pp. 234–237. [CrossRef]

52. Roongmuanpha, N.; Pukkalanun, T.; Tangsrirat, W. Practical realization of electronically adjustable universal filter using commercially available IC-based VBDA. *Eng. Rev.* **2021**, *41*, 1–9. [CrossRef]

53. Jaikla, W.; Siripongdee, S.; Khateb, F.; Sotner, R.; Silaphan, P.; Suwanjan, P.; Chaichana, A. Synthesis of Biquad Filters using Two VD-DIBAs with Independent Control of Quality Factor and Natural Frequency. *AEU Int. J. Electron. Commun.* **2021**, *132*, 153601. [CrossRef]

54. Faseehuddin, M.; Albrni, M.; Sampe, J.; Ali, S.H.M. Novel VDBA based universal filter topologies with minimum passive components. *J. Eng. Res.* **2021**, *9*, 110–130. [CrossRef]

55. *IEEE Recommended Practice and Requirements for Harmonic Control in Electric Power Systems*; IEEE Std 519-2014 (Revision of IEEE Std 519-1992); IEEE: Dallas, TX, USA 2014; pp. 1–29; doi: 10.1109/IEEESTD.2014.6826459. [CrossRef]

56. Tsividis, Y.; McAndrew, C. *Operation and Modeling of the MOS Transistor*; Oxford University Press: Oxford, UK, 2011.

57. Filanovsky, I.; Allam, A. Mutual compensation of mobility and threshold voltage temperature effects with applications in CMOS circuits. *IEEE Trans. Circuits Syst. Fundam. Theory Appl.* **2001**, *48*, 876–884. [CrossRef]

58. Roongmuanpha, N.; Faseehuddin, M.; Herencsar, N.; Tangsrirat, W. Tunable Mixed-Mode Voltage Differencing Buffered Amplifier-Based Universal Filter with Independently High-Q Factor Controllability. *Appl. Sci.* **2021**, *11*, 9606. [CrossRef]